water

MDPI

Article

Assessment of Water Stress Conditions in Central Italy by the Use of Ground and Remotely Sensed Weather Datasets

Maurizio Pieri [1,2,*], Marta Chiesi [1], Luca Fibbi [1,2], Piero Battista [1], Andrea Antonini [2], Bernardo Rapi [1], Francesco Sabatini [1], Bernardo Gozzini [1,2] and Fabio Maselli [1]

[1] National Research Council-Institute of BioEconomy, 50019 Sesto Fiorentino (Firenze), Italy
[2] Consorzio LaMMA (Laboratorio di Meteorologia e Modellistica Ambientale per lo Sviluppo Sostenibile), 50019 Sesto Fiorentino (Firenze), Italy
* Correspondence: maurizio.pieri@ibe.cnr.it

Abstract: Aridity and drought, which are determined by climatic and temporary water scarcity, respectively, are important limiting factors for plant gross primary production. These phenomena are commonly assessed and/or monitored by means of weather indices, most of which are based on observations of precipitation and potential evapotranspiration. The estimation of such indices over large areas can be carried out using multiple datasets, i.e., those derived from weather stations, satellite images, and ground radars. The possibility of using interpolated or remotely sensed datasets in place of ground measurements was currently investigated for Tuscany, a region in Central Italy, showing complex and heterogeneous environmental features. The former weather datasets were first evaluated versus corresponding ground measurements. Next, the basic weather variables were combined and cumulated over 30–60 days to yield synthetic indicators of water deficit, which were assessed in the same way. Finally, these indicators were evaluated to predict the soil water conditions of a meadow and an olive grove during the 2021 summer period. The results obtained indicate that the use of the multi-source weather datasets induces only a minor deterioration of the water stress indicators and is therefore efficient to monitor the water status of different ecosystems with high spatial (200 m) and temporal (daily) details.

Keywords: water deficit; LSA-SAF; HSAF; ERAD; DAYMET; Sentinel–2; weather radar

Citation: Pieri, M.; Chiesi, M.; Fibbi, L.; Battista, P.; Antonini, A.; Rapi, B.; Sabatini, F.; Gozzini, B.; Maselli F. Assessment of Water Stress Conditions in Central Italy by the Use of Ground and Remotely Sensed Weather Datasets. *Water* **2022**, *14*, 3101. https://doi.org/10.3390/w14193101

Academic Editor: Adriana Bruggeman

Received: 31 August 2022
Accepted: 28 September 2022
Published: 2 October 2022

1. Introduction

Water is essential for vegetation growth and plays a fundamental role in determining aridity or drought conditions over land areas. In the context of global warming, changes in water availability have great impacts on terrestrial ecosystems and human activities, which must be properly assessed [1].

Aridity, which is a natural permanent imbalance in water availability, is a land characteristic usually defined over relatively long time periods on the basis of the difference between local water provision by precipitation and water demand by potential evapotranspiration [2]. Arid and semi-arid climates are spread over a large part of the earth surface and are further expanding due to the ongoing climate change, which usually implies an increase of temperature and a reduction in precipitation [3]. This is the case for Mediterranean areas, where the summer dry period, which is due to the co-occurrence of high temperatures and low precipitation, is becoming more intense [4]. Climatic studies carried out in this area, in fact, indicate that air temperature is expected to increase between 2 and 4 °C, while precipitation is expected to decrease both in total amounts and in number of rainy days [5].

The assessment of aridity conditions in terrestrial ecosystems is usually performed by the use of specific indices [6]. In particular, the degree of water deficiency can be eval-

uated by the ratio of long-term (often annual) precipitation (PREC) to potential evapotranspiration (ET_0) observations in the same time interval [7]. The PREC/ET_0 ratio, in fact, is a quantitative aridity index (AI), which can approach zero in the desert but can exceed unity in wet climates [8]. Following the definition of the United Nations Environmental Programme (UNEP), an annual AI value below 0.65 is used for classifying drylands or characterizing different subtypes of aridity: hyperarid ($AI < 0.05$), arid ($0.05 \leq AI < 0.2$), semiarid ($0.2 \leq AI < 0.5$), and dry sub-humid ($0.5 \leq AI < 0.65$) [9].

A related concept is that of drought, which corresponds to an unusual, prolonged dry weather period due to the lack of precipitation and can occur anywhere in the world [10]. Unlike aridity, which is a permanent characteristic of regions with low precipitation, drought is a temporary feature and occurs only when precipitation falls appreciably below the climatic average. The impacts of drought must therefore be seen as dynamic, resulting from interactions between water supply and demand. From a disciplinary perspective, four drought types are usually defined: meteorological, agricultural, hydrological, and socio-economic drought [11,12]. Hence, drought is a complex phenomenon, and even if it is closely related to lack of water in the ground, it is not directly measurable by a single physical variable [13].

Drought conditions, however, can be also described by indicators or parameters, such as precipitation, temperature, evapotranspiration, and soil moisture. Drought indices allow to identify, prevent, or mitigate the conditions and impacts of drought events at the most varied spatio-temporal scales, and they are used in drought early warning systems. A large collection of these indices, classified according to the degree of difficulty of application, is reported in the Handbook of Drought Indicators and Indices [14]. Widely used indices for meteorological and agricultural droughts are described in [13,15,16].

Among these indices, the previously described PREC/ET_0 ratio can be cumulated over shorter time periods (mostly one to few months) in order to effectively define transient water stress conditions, particularly in Mediterranean areas. This is the case for the water stress index proposed by [17], which is derived from the ratio of PREC over ET_0 cumulated over one and two months for grasses and trees, respectively. This index is specifically related to the soil water conditions, which can limit plant transpiration and photosynthesis and can therefore be used to incorporate the effects of water deficit in the estimation of land water and carbon cycles [17–19].

As can be easily understood, the assessment of this or similar indices over wide areas requires the estimation of ET_0 and precipitation with sufficient spatial and temporal resolutions. This task encounters different levels of complexity for the two basic weather variables. Relatively accurate estimates of ET_0, in fact, can be derived from observations of temperature and solar radiation, which are interpolated or extrapolated quite effectively by various techniques. An example is given by the interpolation of daily temperature measurements by statistical tools such as the DAYMET algorithm [20], which has been effectively applied in central Italy by [21]. Solar radiation can instead be predicted using semi-empirical methods based on observations from meteorological satellites [22].

The case is different for precipitation, which is extremely variable both in space and in time and is more complexly linked to the main land features, such as orography, continentality, etc. This makes the inter/extrapolation of precipitation quite difficult to perform without the use of extremely dense networks of rain gauges, which are not always available. This issue actually affects the gridded precipitation datasets produced by such techniques, as the Pan-European E–OBS product, which has been evaluated in Italy both at national and regional scales [23,24]. A valid alternative could be represented by precipitation observations taken by ground-based weather radars, which are now available in a pre-processed format.

These different datasets could therefore be combined to predict land water deficit with sufficient spatial detail (few hundred meters) and temporal frequency (daily). The current paper assesses this possibility by examining the combination of datasets measured on the ground and derived from remote sensing platforms. The study was performed in

a region of central Italy (Tuscany), whose extremely complex and irregular environmental features represent a particular challenge for estimating the spatio-temporal evolution and the impact of water deficit phenomena.

The paper is organized as follows. First, the main features of the study region are introduced, together with the ground and remote sensing data used. The following sections describe the processing steps applied and the results obtained. Finally, discussion and conclusion sections report on the critical issues of the study and on the prospects for future activities.

2. Materials and Methods

2.1. Study Area

Tuscany (42°–45° north latitude and 8°–13° east longitude) is a region situated in central Italy (Figure 1). Its territory is characterized by the presence of hilly areas (about 66% of the whole territory) and mountain zones (about 25%), with altitude varying from 0 to about 2100 m above sea level (i.e., Monte Prado, 2054 m a.s.l.). The climate is consequently very variable, ranging from Mediterranean warm to cool temperate, following the latitudinal and altitudinal gradients and the distance from the sea. The mean annual temperature ranges from about 16.5 °C in the southern plains to 10.5 °C in the mountainous areas; the mean annual precipitation varies from about 450 mm in the south to more than 2000 mm in the north, reaching its maximum on the north-western Apuan Alps [25]. About half of the regional territory is occupied by forests, while the rest is covered by agricultural lands (mostly annual crops in the plains and olive groves/vineyards on the hills) and urban areas.

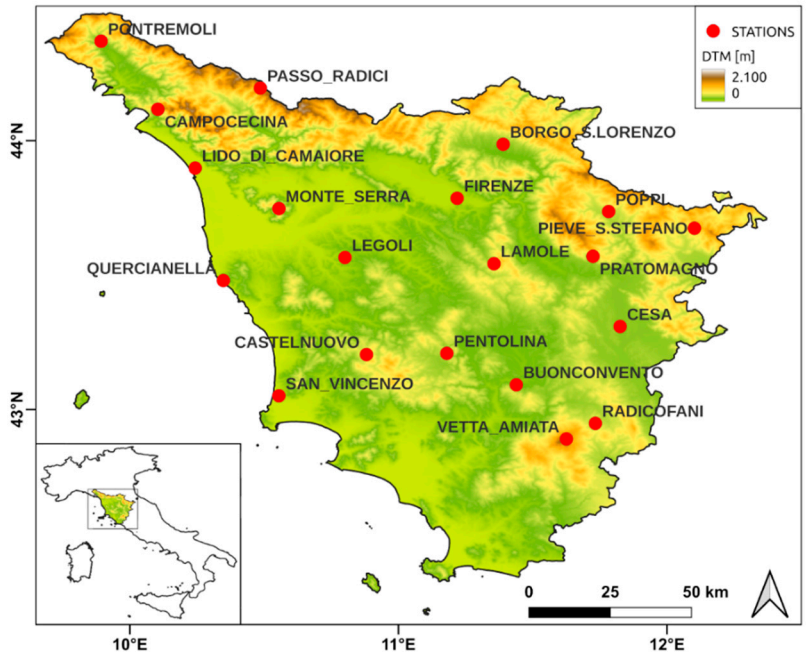

Figure 1. Digital elevation model of the study region (Tuscany) with position of the 20 weather stations considered (red dots). The lower left box shows the position of Tuscany in Italy.

A specific experiment was conducted in a meadow and an olive grove located within the urban park of Cascine (Firenze, Figure 2) [26]. This area is close to the Arno River, at an altitude of about 45 m a.s.l.. The climate is temperate sub-humid, with mean annual precipitation around 800 mm and mean annual temperature of about 15 °C; precipitation is concentrated in autumn and spring, while summer is usually hot and dry. The soil is sandy clay loam (i.e., 52% sand, 24% silt, and 24% clay) and has a depth over 2 m. The

meadow, which is about 30×40 m² wide, is usually grown with spontaneous herbaceous species, while in the olive grove, which extends over about 80×55 m², trees are 5×5 m spaced and have a height around 4 m. Both fields are rainfed and managed following local agricultural habits.

(a)

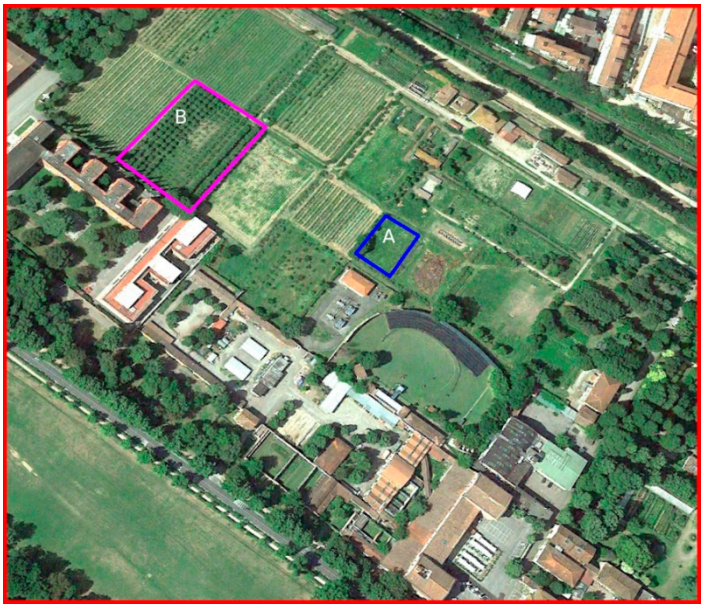

(b)

Figure 2. (**a**) Sentinel-2 MSI NDVI image of June 2021 showing the position of the meadow (blue) and the olive grove (violet) within the Cascine urban Park in Firenze; (**b**) Google Earth true colour composite taken in June 2021 showing the position of the SWC probes within the meadow (**A**) and the olive grove (**B**).

2.2. Study Data

2.2.1. Ground Meteorological Data

Daily meteorological data (i.e., minimum and maximum air temperature, precipitation, and solar radiation) were taken from twenty ground weather stations distributed over the entire regional territory as shown in Figure 1. These stations were selected to cover all local geographical, morphological, and climatic heterogeneities of the region (Table 1). The station of Firenze is placed within the urban park of Cascine (Figure 2). Data were collected from March to November 2021 to be consistent with the period for which radar data are available.

Table 1. Main features of the 20 selected ground weather stations. Mean air temperature and total precipitation refer to the investigated study period, i.e., March–November 2021.

Station ID	Name	Geographical position (° Lat N, ° Long. E)	Elevation (m a.s.l.)	Temperature (°C)	Precipitation (mm)
1	Firenze	43.785, 11.218	40	18.4	421
2	Lido di Camaiore	43.898, 10.243	5	17.1	519
3	San Vincenzo	43.051, 10.555	11	17.8	271
4	Legoli	43.565, 10.801	180	17.8	331
5	Buonconvento	43.092, 11.439	188	17.0	211
6	Quercianella	43.480, 10.348	244	18.6	266
7	Cesa	43.309, 11.825	246	16.3	297
8	Borgo S. Lorenzo	43.986, 11.390	280	15.9	508
9	Pontremoli	44.370, 9.893	340	15.9	874
10	Poppi	43.736, 11.783	417	16.3	424
11	Pentolina	43.210, 11.180	450	17.0	536
12	Lamole	43.542, 11.355	536	15.9	477
13	Radicofani	42.948, 11.733	618	16.4	275
14	Pratomagno	43.570, 11.724	695	15.6	430
15	Pieve S. Stefano	43.674, 12.102	750	13.7	534
16	Castelnuovo Val di Cecina	43.204, 10.881	770	14.5	482
17	Monte Serra	43.747, 10.555	890	13.7	670
18	Campocecina	44.116. 10.104	960	13.7	984
19	Passo delle Radici	44.195, 10.486	1612	8.0	1116
20	Monte Amiata	42.890, 11.625	1678	8.9	454

2.2.2. Ancillary Data

A digital elevation model (DEM) of Tuscany was derived from the database of the LaMMA Consortium; this DEM has a spatial resolution of about 200 m.

Daily soil water content (SWC) measurements were taken both within the olive grove and in the meadow at the Cascine site (Figure 2). The former measurements were collected by means of a Sentek probe (Sentek Sensor Technologies Stepney, Australia) at 0.3 m depth during the period from May to November 2021, while the latter were collected at 0.15 m soil depth by means of a Meter 10HS probe (Meter, Pullman, Washington, USA) from March until November of the same year.

2.2.3. Satellite Data

High spatial resolution (10 m) MultiSpectral Instrument (MSI) images acquired by the twin Copernicus Sentinel-2 (S-2) A and B satellites were utilized to produce the used NDVI imagery. All available MSI images of 2021 covering the Cascine site (Figure 2) were downloaded in an ortho-rectified, pre-processed L2A format from the European Space Agency website (https://sentinel.esa.int/web/sentinel/sentinel-data-access; accessed on 30 August 2022). These images were further processed by performing a maximum value composite (MVC) operation over 15-day periods and by applying two filtering operations aiming at reducing residual disturbances. More specifically, a spatial filtering was applied to remove isolated pixels having anomalous NDVI values; next, a temporal filtering based on an upper envelope algorithm was applied to further reduce atmospheric effects (see [27] for further details).

The spinning-enhanced visible and infrared imager (SEVIRI) images, generated by Meteosat second-generation (MSG) geostationary meteorological satellite, were used to estimate daily solar radiation. These images are provided by the European Organization

for the Exploitation of Meteorological Satellites (EUMETSAT)—Satellite Application Facility on Land Surface Analysis (LSA SAF, https://landsaf.ipma.pt/; accessed on 30 August 2022). The currently used total and diffuse downward surface shortwave flux (MDSSFTD, LSA-207) product is updated every 15 minutes and provides images of DSSF reaching the Earth's surface with a resolution of 3 km at nadir and about 4 x 6 km over Italy [28,29].

Daily precipitation fields were derived from EUMETSAT on Support to Operational Hydrology and Water Management (HSAF, http://hsaf.meteoam.it/; accessed on 30 August 2022). In particular, the accumulated precipitation product (H61B, P-AC-SEVIRI-PMW) obtained by blended MSG data with various low Earth orbit (LEO) satellites was used. The H61B product integrates the instantaneous precipitation maps generated every 15 minutes by the H60B product [30,31]. The original resolution of these products is the same of the MSG imagery.

2.2.4. Radar Data

Radar data obtained from the Italian national ground-based weather radars network were used as 2D precipitation fields. This network is managed by the national Civil Protection Department (DPC). Currently, the network consists of 21 radars distributed throughout the entire Italian territory with several overlapping coverage areas. The weather radars are managed by national and regional institutions including the DPC, the regional weather services, the National Aviation Authority, and the Italian Air Force [32,33].

The raw radar data, according to a shared synchronized schedule, were acquired by various systems and sent to the Central Functional Centre (CFC) of DPC in Rome, where they were merged (mosaicking process) to generate several derived products covering the entire national territory. The products generated every 5 minutes were distributed as georeferenced data grids (at 1 km spatial resolution), by, for example, the portal website: https://radar.protezionecivile.it/radar-dpc (accessed on 30 August 2022).

All products are the result of operational chains that merge radar data with those of the rain gauge network and data from other instruments (e.g., satellite data, lightning strikes, etc.). The instantaneous precipitation data are then cumulated in surface rainfall total (SRT) products for different time interval (1, 3, 6, 12, and 24 hours). All these products were obtained considering the data acquired in real time by the weather stations (about 3000 stations) and available at CFC. A further correction was performed on cumulative precipitation data by combining SRT products with rain gauge observations through a modified conditional merging approach; the resulting rainfall fields are SRTadj [34,35].

The daily cumulative data (expressed in solar time) used in this work were obtained from the hourly SRT1adj and resampled to 200 m spatial resolution for the study area.

2.3. Data Processing

The regional weather datasets currently used were created by the application of different procedures depending on the parameter to consider. All data referred to the period March–November 2021.

Daily minimum and maximum temperatures were interpolated by the application of the DAYMET algorithm [20]. This algorithm is based on the spatially weighted regression concept, i.e., the closer is the observation to the estimation point, the higher its weight, and includes a relationship with elevation, which is derived from the DEM of the region. The application of DAYMET over Tuscany was performed as described in [21].

Daily solar radiation was estimated by the application of the ERAD algorithm [22]. ERAD is based on the disaggregation of DSSF data by DEM and was applied to the entire Italian territory with a time step of 1 min and a spatial resolution of about 200 m. Recently, this methodology was modified to accept as input the new MDSSFTD LSA-207 in place of the LSA-201 product, thus avoiding the need to compute the fraction of diffuse solar radiation.

Daily precipitation estimates were derived from the ground radar observations and, in case of missing data, from the HSAF satellite images, both resampled to the spatial resolution of 200 m.

All these ground, interpolated, and remotely sensed datasets were used to perform three kinds of statistical analysis, which are described in the following paragraphs.

2.3.1. Estimation and Assessment of Daily Precipitation

The first analysis concerned the daily precipitation maps obtained from the remotely sensed data, i.e., the radar observations and the HSAF images. The precipitation estimates were extracted from the pixels corresponding to the 20 weather stations and assessed versus the respective measurements by means of common accuracy statistics, i.e., the determination coefficient (r^2), the root mean square error (RMSE), and the mean bias error (MBE).

2.3.2. Estimation and Assessment of AW

The second analysis was aimed at evaluating the impact of the combined weather dataset on the computation of the water stress factor proposed by [17]. This factor, named available water (AW), is obtained from the ratio between precipitation and potential evapotranspiration as:

$$AW = PREC / ET_0 \quad (1)$$

where PREC is precipitation, and ET_0 is potential evapotranspiration computed on the basis of mean air temperature and solar radiation [36]; both terms are cumulated over one moth for grasses and two months for trees. The theoretical background at the basis of these choices are related to the different behaviours of these plant functional types (e.g., grasses are more quickly affected by soil water shortage than trees because they have limited access to deep storage); more details on this issue can be found in [17] and [37]. As fully described in the same papers, the computation of the final water stress coefficient, named Cws, implies the bounding of AW to 1 and its rescaling between 0 and 0.5. In this way, Cws accounts for the possible impact of water stress on major ecosystem processes (actual evapotranspiration and gross primary production), reducing them to half of their potential value occurring in fully watered conditions [17,18].

Following this theoretical basis, AW over 30 and 60 days cumulation periods were computed for the 20 weather stations using both the ground measurements and the interpolated plus remotely sensed (hereinafter called combined) datasets; the accuracy of the latter was evaluated by inter-comparing the two data series and summarized by means of r^2 and MBE statistics.

2.3.3. Estimation and Assessment of RSWC for Grass and Olive Trees

The third analysis was focused on the prediction of relative soil water content (RSWC), defined as the SWC normalized between possible minimum and maximum values. This indicator is functionally equivalent to the soil water stress coefficient (Ks) described in the Food and Agriculture Organization Paper No. 56 (FAO–56) by [38]. Specifically, the analysis was aimed at evaluating the impact of the combined dataset on the estimation of RSWC in different ecosystems.

To accomplish this task, reference daily RSWC values were obtained from SWC measurements taken within the meadow and the olive grove in the Cascine area. This conversion was carried out as fully described in [39] considering different effective soil depths, i.e., around 0.4 m for the meadow and 1 m for the olive grove.

The estimation of the same quantity was instead performed by applying the method proposed by [19] to the combined datasets. That method predicts daily RSWC by weighting the AW factors of vegetation and soil for the respective cover fractions:

$$RSWC = FVC\ (0.5 + 0.5\ AW) + (1 - FVC)\ AW \quad (2)$$

Within this formulation, the fractional vegetation cover (FVC) is considered to be responsive to the soil water condition integrated over a sufficient time period (one or two months) and was consequently used to modulate the intensity of SWC variations. Equation (2) was therefore applied to estimate the RSWC for the Cascine meadow and olive grove deriving the respective FVC from the NDVI MSI images, as fully described in [24]. The AW meteorological factors were computed using both the ground and combined datasets cumulated over 1 or 2 months, respectively. The accuracy of the two estimated series was finally assessed versus the reference RSWC observations using the same statistics as above.

3. Results

3.1. Daily Precipitation Estimates

The combination of radar and HSAF precipitation data yields a complete daily dataset over the entire regional territory. Fortunately, in fact, only few radar precipitation observations are missing during the study period, and in all these cases, HSAF estimates are present.

Table 2 shows the accuracy statistics obtained comparing the precipitation measurements collected at the 20 weather stations to the corresponding remotely sensed estimates. Most determination coefficients are higher than 0.63, while seven coefficients vary between 0.27 and 0.57. The lowest correlation is obtained for a mountain station (Passo delle Radici), which is also characterized by high errors. In general, the accordance between daily measurements and estimates is moderate for all stations, with a mean determination coefficient of 0.52 and a slight tendency to underestimation (the mean MBE is 0.27 mm).

Table 2. Accuracy statistics of the remotely sensed daily precipitation estimates for the 20 ground weather stations over the study period (March–November 2021).

Station ID	Name	r^2	RMSE (mm)	MBE (mm)
1	Firenze	0.695	2.83	0.45
2	Lido di Camaiore	0.499	4.72	−1.00
3	San Vincenzo	0.694	2.26	0.02
4	Legoli	0.691	2.30	−0.25
5	Buonconvento	0.689	3.11	0.66
6	Quercianella	0.673	2.40	0.16
7	Cesa	0.637	2.08	0.19
8	Borgo S. Lorenzo	0.672	2.78	−0.23
9	Pontremoli	0.661	6.52	−0.57
10	Poppi	0.661	2.52	0.11
11	Pentolina	0.792	4.45	−0.14
12	Lamole	0.495	3.86	−0.91
13	Radicofani	0.718	1.77	0.32
14	Pratomagno	0.652	2.92	0.13
15	Pieve S. Stefano	0.572	3.47	−0.16
16	Castelnuovo Val di Cecina	0.510	4.12	−0.26
17	Monte Serra	0.635	4.51	−1.18
18	Campocecina	0.515	8.14	−0.85
19	Passo delle Radici	0.266	10.41	−1.12
20	Monte Amiata	0.361	4.31	−0.76

3.2. AW Estimates

The daily evolutions of the AW computed for grass and olive trees at the Cascine site using the ground and the combined meteorological data are shown in Figure 3. These water stress factors follow a pattern that is typical for Mediterranean areas, being lowest during the hot and dry summer and having a complete recovery during late autumn.

The different behaviour of grass with respect to olive trees is reflected by the more marked and frequent variations in water status characterizing the former plant functional type. The use of the combined data in place of the ground meteorological data does not induce significant differences in the AW estimates, with the determination coefficient equal to 0.945 and 0.980 for grass and olive trees, respectively; both errors are also low (i.e., RMSE = 0.093 and MBE = −0.003 for grass and RMSE = 0.056 and MBE = −0.007 for olive trees).

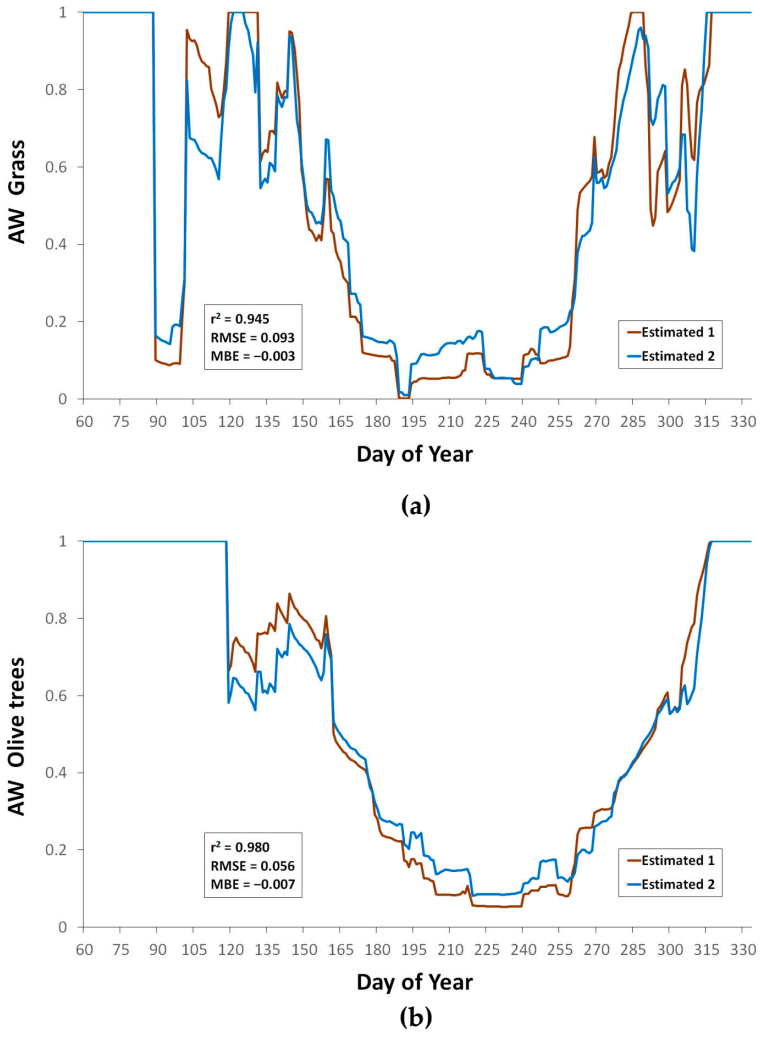

Figure 3. Daily evolutions of AW obtained from ground (Estimated 1) and combined (Estimated 2) meteorological data, computed from March to November 2021 for grass (**a**) and olive trees (**b**) at the Cascine site (all correlations are highly significant, $p < 0.01$).

Figure 4a shows the determination coefficients obtained from the same intercomparisons for all 20 study stations. As expected, the accordance between reference and estimated AW computed over one month is slightly lower than that computed over two months due to the greater smoothing induced by the latter operation; the same is mostly the case for the mean bias errors (Figure 4b). On average, there is a slight tendency to underestimation, which derives from the corresponding precipitation pattern seen before.

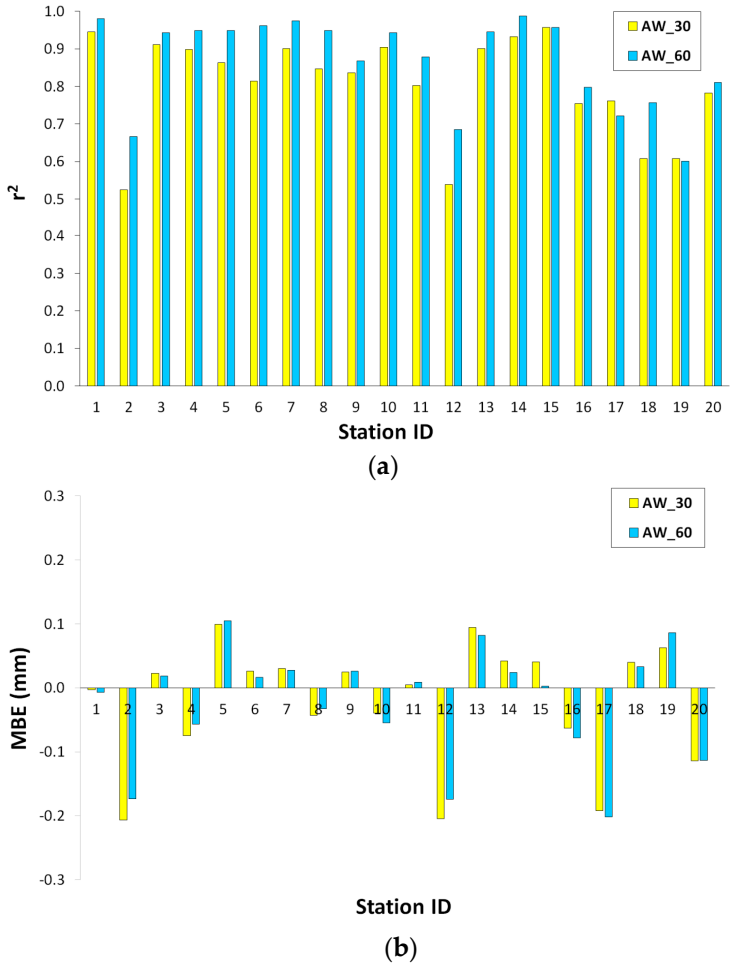

Figure 4. Histograms showing the determination coefficient (r^2) (**a**) and the mean bias error (MBE) (**b**) computed between AW computed over 30 and 60 days using ground and combined meteorological data (all correlations are highly significant, $p < 0.01$).

Figure 5 illustrates the spatial distribution of the AW factor obtained using the combined dataset for the driest period of 2021, i.e., July–August. The highest values are concentrated in the north-west of the region, which corresponds to a particularly rainy and humid mountain zone, the Apuan Alps. Very low AW values characterize most Tuscany plains, especially near the coastline, where summer rainfalls are scarce.

3.3. RSWC estimates

Figure 6 shows the reference RSWC evolutions of the Cascine meadow and olive grove. The different trends of the two vegetation types are mostly due to the respective soil depths considered (0.4 and 1.0 m) and highlight their different responses to summer water stress, with the RSWC of grass being lower and more variable than that of olive trees.

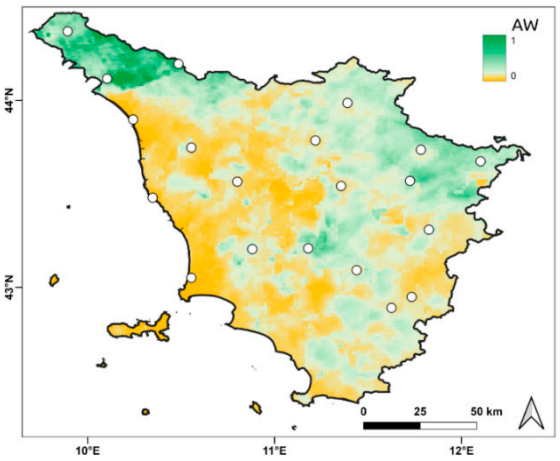

Figure 5. AW map of Tuscany obtained using the combined dataset for July–August 2021, with position of the 20 weather stations considered (white dots).

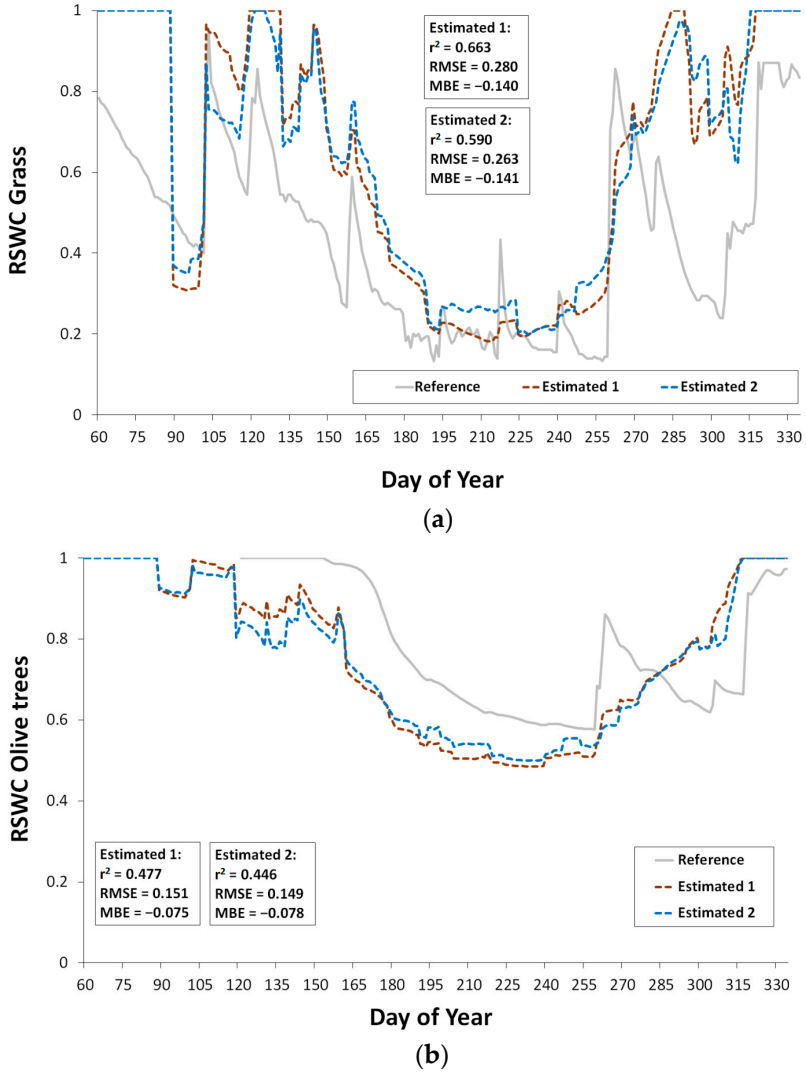

Figure 6. Reference RSWC evolutions compared to the estimates obtained using ground (Estimated 1) and combined (Estimated 2) meteorological data for grass (**a**) and olive trees (**b**) at the Cascine site (all correlations are highly significant, $p < 0.01$).

These RSWC patterns are also partly responsible for the different FVC evolutions of grass and olive trees, which are visible in Figure 7. Grass shows an FVC decrease from the initial level of about 0.6 until a minimum close to 0.25 in the middle of summer. This is followed by a clear recovery during autumn, which leads to values close to 0.8. On the contrary, olive trees, which are evergreen, have a nearly stable FVC during the whole year.

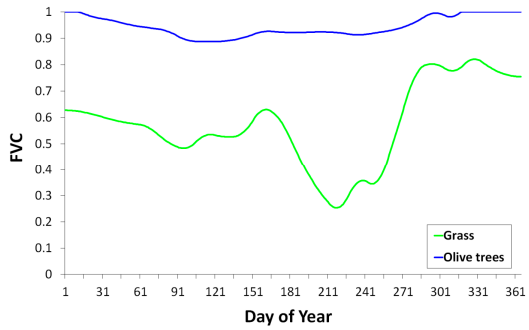

Figure 7. FVC evolutions of grass and olive trees at the Cascine site obtained from Sentinel-2 MSI NDVI images during the year 2021.

The application of Equation (2) to these FVC and the AW values of Figure 3 yields the RSWC estimates shown again in Figure 6 for the meadow (a) and the olive grove (b). In the former case, the estimated RSWC is lower than 1 during some spring and fall dry spells, and the minimum values (<0.2) are found in July and August, partly due to the summer FVC drop. Similar patterns are predicted using the ground and the combined meteorological datasets; in both cases, the determination coefficient between reference and estimated RSWC is higher than 0.59, and the errors are comparably low.

The seasonal RSWC evolution predicted for olive trees is slightly different: its values are close to the maximum till the middle of June; after that, they slowly decrease until a minimum, which is around 0.6 at the end of summer. A first recovery then occurs, which is not sufficient to completely restore the spring values. The use of the ground and combined datasets still produces similar estimates both in terms of correlation and errors.

4. Discussion

Water stress has a potentially relevant impact on all aspects of plant growth, among which a decrease in plant size, leaf area, and biomass is the most immediate. Judging whether plants are suffering for a water shortage should start from the consideration of all involved eco-physiological factors, namely soil, climate, and plant conditions. Therefore, the assessment of water stress effects over large areas is a relevant issue not easily achievable using only conventional measurements that are collected over limited areas and can represent only local conditions.

Valuable alternatives can be offered by the use of interpolated and remotely sensed datasets, the latter obtained from satellites or ground radars: by means of these, in fact, spatial and synoptic information over large areas can be obtained through limited processing and the application of strong methodologies [40–42].

The extension of meteorological data over large areas is usually based on interpolation/extrapolation methods that have been widely validated and applied. For instance, in the study region, the estimation of daily minimum and maximum air temperature was performed by the application of the DAYMET algorithm [20], which yielded limited errors and generally satisfactory results [21].

As regards solar radiation, the currently applied ERAD algorithm, which is based on the use of Meteosat images, has been recently assessed all over Italy against independent ground measurements [22]. As previously noted, the current use of this algorithm required a slight modification to accept the new DSSF product (i.e., the LSA-207 in place of the previous LSA-201 version).

The main novelty of the present investigation concerned the use of precipitation estimates obtained from the national radar network. As previously noted, these estimates are expected to provide a decisive step forward with respect to satellite products such as HSAF due to their sounder physical basis and their higher spatial and temporal resolutions. This expectation was actually confirmed by the current experimental findings, which indicated a notable superiority of the radar over the HSAF precipitation estimates (data not shown).

Nevertheless, the radar estimates are still affected by various shortcomings, which should at least be properly known. Since the weather radars predict precipitation through the reflectivity in altitude, errors and uncertainty can arise both from the basic measurement of reflectivity and from attempts to relate this to the precipitation actually falling at the ground [43]. Moreover, in some areas, the radar coverage can be suboptimal to retrieve a good representativeness of the whole territory, especially in mountainous areas where the radar beam might be intercepted by the ground [44]. In case of the precipitation product SRTadj, however, the impact of these shortcomings is mitigated by the continuous adjustment that is routinely performed versus rain gauge measurements, which allows for a more reliable quantitative estimation of the areal distribution of precipitation.

A secondary issue concerns the spatial resolution of the original radar dataset, which is about 1 km. This required a resampling of the estimates to the common resolution of the other meteorological parameters, i.e., 200 m, the impact of which is difficult to assess. An additional problem is related to possible missing values, which was currently overcome by combining the radar with the corresponding HSAF estimates.

When evaluated versus rain gauge measurements, the combined precipitation estimates obtained show an accuracy that is comparable to that found by [35] in their assessment of the same dataset over the entire Italian national territory. Such accuracy is sufficient for most operational applications and particularly for the prediction of water stress conditions over wide Mediterranean areas. This is confirmed by the final tests performed, which demonstrate that the use of the combined precipitation estimates allows to yield efficient spatialized indicators of both meteorological and soil water stress conditions.

5. Conclusions

The current work has produced and assessed a daily dataset informative on drought conditions in Tuscany (central Italy). The dataset was obtained by combining interpolated values of temperature with satellite-based simulations of solar radiation and ground radar estimates of precipitation. A comparison with the data collected by rain gauges all over the region demonstrates that the precipitation estimates reproduce the ground observations quite faithfully. This property is further enhanced by the composition of the estimates with ET_0 observations for the definition of water stress conditions over one two-month periods. As expected, in fact, the use of these relatively long cumulation periods has a positive impact on the accuracy of the meteorological water stress indicators.

The ecological relevance of these indicators has been demonstrated in numerous previous publications [17,18], which have shown their efficiency for characterizing the impact of water stress on major vegetation processes (i.e., transpiration and photosynthesis). The meteorological information brought by these indicators can be combined with remotely sensed estimates of vegetation status for predicting soil water conditions, i.e., RSWC. This indicator, or its analogous FAO–56 water stress coefficient Ks, is decisive for regulating plant photosynthetic activity in arid and semi-arid regions [45]. This enhances the importance of the findings obtained at the Cascine experimental site, where a meadow and an olive grove were monitored by means of soil water capacitive probes and a ground meteorological station. The results of this experiment confirm that the use of the combined weather datasets induces only a minor deterioration in the prediction of RSWC for both ecosystem types.

It can therefore be concluded that these datasets can be properly utilized to assess the water stress condition of different ecosystems in Tuscany as well as in similar environmental situations.

Author Contributions: M.P., M.C., A.A. and F.M. conceived the structure and wrote the manuscript. L.F., P.B., B.R., F.S. and B.G. differently contributed to the collection and analysis of the ground and remotely sensed datasets utilized. All authors have read and agreed to the published version of the manuscript.

Funding: This research received no external funding.

Data Availability Statement: The data used in this study are available from the corresponding authors upon request.

Acknowledgments: The authors wish to thank the "Istituto Tecnico Agrario" of Firenze for offering the experimental site. Three anonymous *Water* reviewers are thanked for their helpful comments on the first draft of the manuscript.

Conflicts of Interest: The authors declare no conflict of interest.

References

1. Gudmundsson, L.; Greve, P.; Seneviratne, S.I. The sensitivity of water availability to changes in the aridity index and other factors—A probabilistic analysis in the Budyko space. *Geophys. Res. Lett*. **2016**, *43*, 6985–6994.
2. Pereira, L.S.; Oweis, T.; Zairi, A. Irrigation management under water scarcity. *Agric. Water Manag.* **2002**, *57*, 175–206.
3. Wang, T.; Tu, X.; Singh, V.P.; Chen, X.; Lin, K. Global data assessment and analysis of drought characteristics based on CMIP6. *J. Hydrol.* **2021**, *596*, 126091.
4. Barredo, I.; Caudullo, G.; Dosio, A. Mediterranean habitat loss under future climate conditions: Assessing impacts on the Natura 2000 protected area network. *Appl. Geogr.* **2016**, *75*, 83–92.
5. Giorgi, F.; Raffaele, F.; Coppola, E. The response of precipitation characteristics to global warming from climate projections. *Earth Syst. Dynam*. **2019**, *10*, 73–89.
6. Ullah, S.; You, Q.; Sachindra, D.A.; Nowosad, M.; Ullah, W.; Bhatti, A.S.; Jin, Z.; Ali, A. Spatiotemporal changes in global aridity in terms of multiple aridity indices: An assessment based on the CRU data. *Atmos. Res.* **2022**, *268*, 105988.
7. Zhang, C.; Yang, Y.; Yang, D.; Wu, X. Multidimensional assessment of global dryland changes under future warming in climate projections. *J. Hydrol.* **2021**, *592*, 125618.
8. Fu, Q.; Feng, S. Responses of terrestrial aridity to global warming. *J. Geophys. Res. Atmos*. **2014**, *119*, 7863–7875.
9. Yu, H.; Zhang, Q.; Wei, Y.; Liu, C.; Ren, Y.; Yue, P.; Zhou, J. Bias-corrections on aridity index simulations of climate models by observational constraints. *Int. J. Climatol.* **2022**, *42*, 889–907.
10. Wilhite, D.A. Chapter 1 Drought as a Natural Hazard: Concepts and Definitions. In *Drought: A Global Assessment*; Wilhite, D.A., Ed.; Drought Mitigation Center Faculty Publications, 69; Routledge: London, UK, 2000; Volume I, pp. 3–18.
11. Wilhite, D.A.; Glantz, M.H. Understanding the Drought Phenomenon: The Role of Definitions. *Drought Mitig. Cent. Fac. Publ.* **1985**, *20*, 110–120.
12. Van Loon, A.F. Hydrological drought explained. *WIREs Water* **2015**, *2*, 359–392.
13. Hološ, S.; Šurda, P. Evaluation of drought—Review of drought indices and their application in the recent studies from Slovakia. *Acta Hortic. Et Regiotect. Spec. Issue* **2021**, *24*, 97–108.
14. Svoboda, M.; Fuchs, B. Integrated Drought Management Programme (IDMP). In *Handbook of Drought Indicators and Indices*; Drought Mitigation Center Faculty Publications, 117; World Meteorological Organization: Geneva, Switzerland, 2016.
15. Cammalleri, C.; Arias-Munoz, C.; Barbosa, P.; De Jager, A.; Magni, D.; Masante, D.; Mazzeschi, M.; McCormick, N.; Naumann, G.; Spinoni, J.; et al. A Revision of the Combined Drought Indicator (CDI) used in the European Drought Observatory (EDO). *Nat. Hazards Earth Syst. Sci.* **2021**, *21*, 481–495.
16. Azman, R.M.N.R.; Noor, N.A.M.; Abdullah, S.; Mohamed, M. A review on the assessment of drought index. *Gading J. Sci. Technol.* **2022**, *5*, 59–68.
17. Maselli, F.; Papale, D.; Puletti, N.; Chirici, G.; Corona, P. Combining remote sensing and ancillary data to monitor the gross productivity of water-limited forest ecosystems. *Remote Sens. Environ*. **2009**, *113*, 657–667.
18. Maselli, F.; Papale, D.; Chiesi, M.; Matteucci, G.; Angeli, L.; Raschi, A.; Seufert; G. Operational monitoring of daily evapotranspiration by the combination of MODIS NDVI and ground meteorological data: Application and validation in Central Italy. *Remote Sens. Environ.* **2014**, *152*, 279–290.
19. Gardin, L.; Chiesi, M.; Fibbi, L.; Angeli, L.; Rapi, B.; Battista, P.; Maselli, F. Simulation of soil water content through the combination of meteorological and satellite data. *Geoderma* **2021**, *393*, 115003.

20. Thornton, P.E.; Running, S.W.; White, M.A. Generating surfaces of daily meteorological variables over large regions of complex terrain. *J. Hydrol.* **1997**, *190*, 214–251.
21. Chiesi, M.; Maselli, F.; Moriondo, M.; Fibbi, L.; Bindi, M.; Running, S. Application of BIOME-BGC to simulate Mediterranean forest processes. *Ecol. Model.* **2007**, *206*, 179–190.
22. Fibbi, L.; Maselli, F.; Pieri, M. Improved estimation of global solar radiation over rugged terrains by the disaggregation of Satellite Applications Facility on Land Surface Analysis data (LSA SAF). *Meteorol. Appl.* **2020**, *27*, e1940.
23. Fibbi, L.; Chiesi, M.; Moriondo, M.; Bindi, M.; Chirici, G.; Papale, D.; Maselli, M. Correction of a 1 km daily rainfall dataset for modelling forest ecosystem processes in Italy. *Meteorol. Appl.* **2016**, *23*, 294–303.
24. My, L.; Di Bacco, M.; Scorzini, A.R. On the use of gridded data products for trend assessment and aridity classification in a Mediterranean context: The case of the Apulia Region. *Water* **2022**, *14*, 2203.
25. Rapetti, F.; Vittorini, S. *Carta Climatica Della Toscana*; Pacini Editore: Pisa, Italy, 1995.
26. Chiesi, M.; Costafreda-Aumedes, S.; Argenti, G.; Battista, P.; Fibbi, L.; Leolini, L.; Moriondo, M.; Rapi, B.; Sabatini, F.; Maselli, F. Estimating the GPP of olive trees with variable canopy cover by the use of Sentinel-2 MSI images. *Eur. J. Agron.* **2022**, *141*, 126618.
27. Maselli, F.; Battista, P.; Chiesi, M.; Rapi, B.; Angeli, L.; Fibbi, L.; Magno, R.; Gozzini, B. Use of Sentinel-2 MSI data to monitor crop irrigation in Mediterranean areas. *Int. J. Appl. Earth Obs. Geoinf.* **2020**, *93*, 102216.
28. Carrer, D.; Ceamanos, X.; Moparthy, S.; Vincent, C.; Freitas, S.C.; Trigo, I.F. Satellite Retrieval of Downwelling Shortwave Surface Flux and Diffuse Fraction under All Sky Conditions in the Framework of the LSA SAF Program (Part 1: Methodology). *Remote Sens.* **2019**, *11*, 2532.
29. Carrer, D.; Moparthy, S.; Vincent, C.; Ceamanos, X.C.; Freitas, S.; Trigo, I.F. Satellite Retrieval of Downwelling Shortwave Surface Flux and Diffuse Fraction under All Sky Conditions in the Framework of the LSA SAF Program (Part 2: Evaluation). *Remote Sens.* **2019**, *11*, 2630.
30. HSAF. *Product Validation Report (PVR) for Products H60B (P-AC-SEVIRI-PMW) and H63 (P-AC-SEVIRI_E)*; SAF/HSAF/PVR-60-63, 2.0; EUMETSAT: Darmstadt, Germany, 27 February 2022; pp. 1–112.
31. HSAF. *Product Validation Report (PVR) for Products P-AC-SEVIRI-PMW (H61B) and P-AC-SEVIRI_E (H90)*; SAF/HSAF/PVR-61-90, 2.0; EUMETSAT: Darmstadt, Germany, 27 February 2022; pp. 1–122.
32. Vulpiani, G.; Pagliara, P.; Negri, M.; Rossi, L.; Gioia, A.; Giordano, P.; Alberoni, P.P.; Cremonini, R.; Ferraris, L.; Marzano, F.S. The Italian radar network within the national early-warning system for multi-risks management. In Proceedings of the Fifth European Conference on Radar in Meteorology and Hydrology (ERAD 2008), Helsinki, Finland, 30 June–4 July 2008; p. 184.
33. Vulpiani, G.; Montopoli, M.; Passeri, L.D.; Gioia, A.G.; Giordano, P.; Marzano, F.S. On the Use of Dual-Polarized C-Band Radar for Operational Rainfall Retrieval in Mountainous Areas. *J. Appl. Meteorol. Climatol.* **2012**, *51*, 405–425.
34. Pignone, F.; Rebora, N.; Silvestro, F.; Castelli, F. GRISO (Generatore Random di Interpolazioni Spaziali da Osservazioni incerte)—Piogge, Relazione delle attività del I anno inerente la Convenzione 778/2009 tra Dipartimento di Protezione Civile e Fondazione CIMA (Centro Internazionale in Monitoraggio Ambientale). *Report* **2010**, *272*, 353.
35. Bruno, G.; Pignone, F.; Silvestro, F.; Gabellani, S.; Schiavi, F.; Rebora, N.; Giordano, P.; Falzacappa, M. Performing hydrological monitoring at a national scale by exploiting rain-gauge and radar networks: The Italian case. *Atmosphere* **2021**, *12*, 771.
36. Jensen, M.E.; Haise, H.R. Estimating evapotranspiration from solar radiation. In *Proceedings of the American Society of Civil Engineers*; Nabu Press: Charleston, SC, USA, 1963; volume 89, pp. 15–41.
37. Maselli, F.; Argenti, G.; Chiesi, M.; Angeli, L.; Papale, D. Simulation of grassland productivity by the combination of ground and satellite data. *Agric. Ecosyst. Environ.* **2013**, *165*, 163–172.
38. Allen, R.G.; Pereira, L.S.; Raes, D.; Smith, M. *Crop Evapotranspiration—Guidelines for Computing Crop Water Requirements*; FAO Irrigation and Drainage Paper 56; Food and Agricultural Organization of the United Nations: Rome, Italy, 1998.
39. Chiesi, M.; Battista, P.; Fibbi, L.; Gardin, L.; Pieri, M.; Rapi, B.; Romani, M.; Maselli, F. A semi-empirical method to estimate actual evapotranspiration in Mediterranean environments. *Adv. Meteorol.* **2018**, *2018*, 9792609.
40. Levizzani, V.; Cattani, E. Satellite Remote Sensing of Precipitation and the Terrestrial Water Cycle in a Changing Climate. *Remote Sens.* **2019**, *11*, 2301.
41. West, H.; Quinn, N.; Horswell, M. Remote sensing for drought monitoring & impact assessment: Progress, past challenges and future opportunities. *Remote Sens. Environ.* **2019**, *232*, 111291.
42. Binetti, M.S.; Campanale, C.; Massarelli, C.; Uricchio, V.F. The Use of Weather Radar Data: Possibilities, Challenges and Advanced Applications. *Earth* **2022**, *3*, 157–171.
43. Sokol, Z.; Szturc, J.; Orellana-Alvear, J.; Popová, J.; Jurczyk, A.; Célleri, R. The Role of Weather Radar in Rainfall Estimation and Its Application in Meteorological and Hydrological Modelling—A Review. *Remote Sens.* **2021**, *13*, 351.
44. Harrison, D.L.; Driscoll, S.J.; Kitchen, M. Improving precipitation estimates from weather radar using quality control and correction techniques. *Meteorol. Appl.* **2000**, *7*, 135–144.
45. Kokkotos, E.; Zotos, A.; Patakas, A. Evaluation of Water Stress Coefficient Ks in Different Olive Orchards. *Agronomy* **2020**, *10*, 1594.